

A novel computerized viscometer/rheometer

Jorge A. Jimenez^{a)} and M. Kostic^{b)}

Department of Mechanical Engineering, Northern Illinois University, DeKalb, Illinois 60115-2854

(Received 11 August 1993; accepted for publication 12 October 1993)

An innovative, Couette-type viscometer/rheometer was developed, designed, and fabricated with the main objective being to measure viscosity and elastic properties of low-viscous, non-Newtonian, and visco-elastic fluids, like dilute polymer solutions. The goal was to simplify and improve some existing drawbacks of commercial instruments employing several novel design solutions, particularly with regard to instrument precision and sensitivity. With a single pair of cylinders and a torsion bar stiffness of 0.116 Nm/rad, viscosities from 0.5 to 50 000 cP (centi-Poise) in a shear-rate range from 1 to 200 s⁻¹, and oscillatory tests from 0.1 to 10 Hz, could be measured. The transducers' electronic signals are handled by a software, developed in C language, and an IBM-PC compatible computer with a data acquisition board. The innovative design solutions (use of a cruciform torsion bar, optoelectronics sensors, and a novel alignment procedure) have improved the critical instrument performance and reduced the number and cost of components, customarily used in commercial viscometers/rheometers. The overall steady shear-rate calibration was performed using the standard-viscosity fluids of 51 and 445 cP. Initial results show high precision (around 4%), particularly at higher velocities. The oscillatory testing was performed by measuring the phase shift between the stress and strain for viscoelastic fluids and for the limiting case of a standard Newtonian fluid. The novel design has proved efficient and with potential for further improvements.

I. INTRODUCTION

A computerized, concentric-cylinders Couette-type viscometer/rheometer was developed to measure viscosity and elastic properties of low-viscous, non-Newtonian aqueous polymer solutions.^{1,2} The instrument will be used for demonstration for senior laboratory and design courses, and as a crucial instrument for a research project on studying flow and heat transfer behavior of non-Newtonian viscoelastic fluids at Northern Illinois University.³⁻⁶ Usually, the commercial rheometers are designed to measure viscous and elastic properties of rather "thick" (high-viscous) fluids. The viscosity, and particularly elastic properties of dilute aqueous solutions, were at the very low end of measurement ranges of these commercial instruments, usually accompanied with unstable operation and lower accuracy in that region. Their price range is anywhere up to \$100 000 or even higher. A more precise and much less costly instrument than the ones commercially available could be developed by using an innovative design described in this paper.

The three basic measurements performed by a viscometer/rheometer are: (1) *torque*, which is correlated to the fluid's shear stress; (2) *rotational velocity*, which is correlated to the fluid's shear strain rate; and (3) *oscillatory motion*, which is correlated to the fluid's strain, and is simultaneously measured with the corresponding torque (or stress) and used for determination of fluid elastic properties. For low-viscous fluids, the stress to be measured is very small, in the order of milli-Newton meters (mNm).

Commercial instruments typically use simple cylindrical or rectangular torsion spring bars and linear variable differential transformers (LVDT) for torque measurements. A small diameter of the torsion bar is needed to provide a low torsional resistance and appropriate resolution for very small torques. Unfortunately, small torsion spring size (diameter) also reduces the bending resistance (i.e., structural rigidity) and therefore, the instrument's operational stability. Ideally, in the case of Couette-type geometry, the stationary inner cylinder should be suspended freely on the torsion spring bar for precise torque measurement. However, such sensitive (and tiny) torsion spring bars could not provide the necessary alignment between the inner and the outer cylinder, nor a stable operation during the testing. This problem is overcome by the use of cumbersome and expensive air bearings. In addition, to ensure a correct alignment, most components are fabricated with very precise tolerances and, therefore, substantially increased cost.

The goal was to simplify and improve some existing drawbacks of commercial instruments employing several novel design solutions, particularly with regard to instrument precision and sensitivity. Three novel solutions have made our viscometer/rheometer distinctive from the commercial ones, with a number of advantages and substantially less expensive. These solutions are: (1) a design of a special cruciform torsion-spring bar; (2) use of very inexpensive, general-purpose optoelectronic sensors; and (3) a special alignment technique and procedure.

There is an additional important benefit of developing your own instrument: a full control over the design and functionality of the instrument. This is essential for a better interpretation of measured fluid properties. Not only the measurement results are known, but the "unrestricted and

^{a)}Presently with Tellabs Operations, Inc., Digital Systems Division, Lisle, Illinois.

^{b)}The author who is continuing with this project and to whom future correspondence should be addressed.

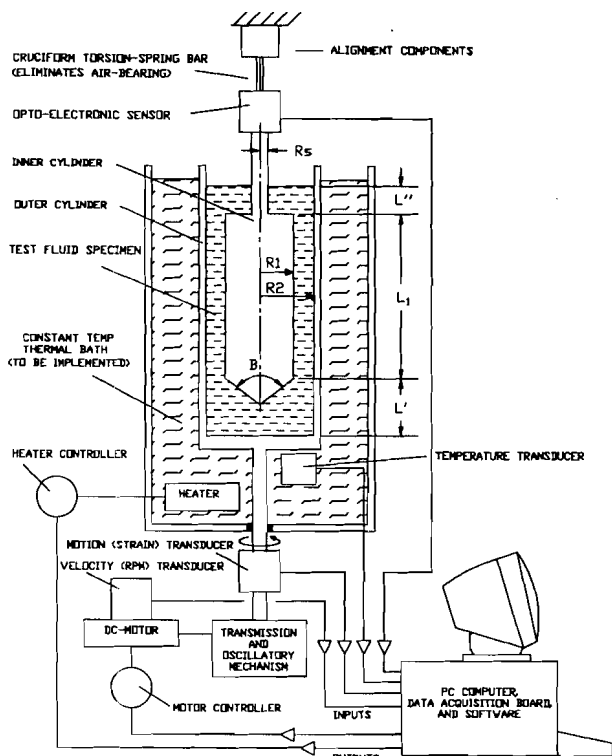


FIG. 1. Instrument schematic with concentric cylinders' dimensions.

inside" conditions and procedure of getting them as well, including the parameters involved in the design and calibration along with the errors related to mechanical and electronic components. An in-house, flexible, and open design also allows for further modifications and improvements.

This viscometer/rheometer was developed for fluid viscosity measurements within a range of 0.5–50 000 mPa s [1 milli-Pascal-second = 1 cP (centi-Poise)] over a shear rate range of 1–200 s⁻¹. Even this range could be extended by providing different cylinders' and torsion bar sizes. The developed viscometer/rheometer is capable of determining elasticity in viscoelastic fluids by measuring the phase lag between stress and strain, and the dynamic (storage and loss) moduli. The goal was to achieve at least 5% accuracy and 3% repeatability. The design allows for the addition of a controlled temperature bath. The DIN German standards, which are followed by most manufacturers of similar instruments, were used for the dimensioning of the cylinders' geometry. Using recognized standards allows for easier and more reliable data reduction and comparison. The viscometer/rheometer has been designed for manufacturability and easy assembly, using standard off-the-shelf components wherever possible.

II. GENERAL DESIGN DESCRIPTION

A schematic diagram of the viscometer is shown in Fig. 1, while the instrument assembly and major mechanical components are presented in Fig. 2. There are two modes of operation: (1) steady rotational mode for viscosity measurement, and (2) oscillatory rotation for elasticity

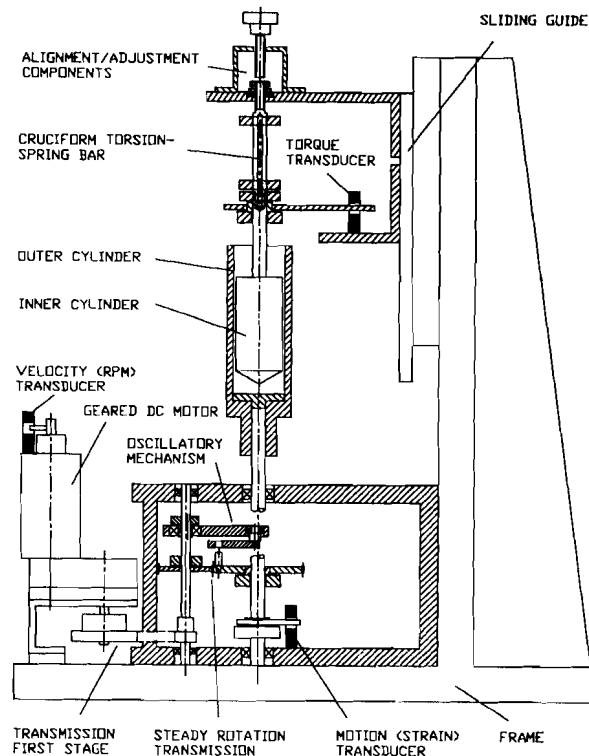


FIG. 2. Instrument assembly and major components.

measurement (phase shift between stress and strain and dynamic moduli). In the first mode, the outer cylinder rotates at controllable constant speeds. In the second mode, the outer cylinder oscillates in a simple harmonic motion (sinusoidally) with preset amplitudes at controllable frequencies. The outer cylinder rotates (Couette-type), continuously deforming a sample test-fluid which then exerts a viscous torque on the stationary inner cylinder. This torque is measured using a specially designed torsion bar, on which the stationary inner cylinder is freely suspended, and an optoelectronic sensor. The rotational velocity of the outer cylinder is measured using an optical switch-counter sensor, mounted on the motor's shaft. The oscillatory motion of the outer cylinder, i.e., the fluid's strain, is measured using an optoelectronic sensor. All sensors' signals are read and controlled through a general-purpose data acquisition board, installed in an IBM-PC compatible computer. Random errors are reduced statistically by taking several measurements of each variable at high sampling frequency.

As already mentioned, Fig. 2 shows the instrument assembly and major mechanical components. A more detailed explanation is given by Jimenez.¹ The frame and other support components were made of aluminum, easy to machine, light, and with good appearance. The motor and transmission are selected knowing the velocity (i.e., shear rate) range, the frequency range, and the expected torque (i.e., viscosity) range. In our design, the velocity range was 1–180 rpm, and the frequency range 0.1–10 Hz. It can be shown that the torque and power requirements are mostly due to viscous effects. Knowing that velocities and accel-

erations are small, inertial forces can be neglected for the motor selection. A geared dc commutator motor was selected because its operation is smoother than a stepper motor and easier to control the velocity than an ac motor.⁷ Also, the electronic voltage controllers are less expensive and complex than electronic frequency controllers.

A special sensor is needed to measure the rotational velocity that varies over a wide range (1–180 rpm). A tachometer, whose voltage is proportional to velocity, would not be very accurate over such a wide range. A slotted optical sensor (interrupter) was chosen to measure the rpm velocity of the motor. It generates an electrical pulse for every revolution of the motor. At the same time, a timer of the data acquisition board generates 5 MHz pulses. Using hardware interrupts, the computer counts the number of 5 MHz pulses between two pulses sent by the slotted optical sensor (or every revolution). The velocity of the outer cylinder can then be calculated easily knowing the transmission ratios: the first stage gear box (1/108.8), pulleys (3/1), and spur gears (3/5), see Fig. 2. For example, at 1 and 180 rpm, the counted number of 5 MHz pulses is 82721 ± 1 and 460 ± 1 , respectively. The motor velocity is controlled by an analog signal from the data acquisition board which is further amplified using operational amplifiers and a Darlington transistor. The other crucial components of the instrument are described in detail in the following sections.

III. CONCENTRIC-CYLINDER GEOMETRY AND THEORY

Concentric-cylinder type viscometer/rheometers are usually employed when absolute viscosity needs to be determined which, in turn, requires knowledge of well-defined shear rate and shear stress data. Such instruments are available in different configurations and can be used for almost any fluid. There are models for low and high shear rates. More complete discussion on concentric-cylinder viscometer/rheometers is given elsewhere.^{8–11} The Couette-type viscometer (the outer cylinder, or cup, rotates) minimizes centrifugal forces, which cause the Taylor vortices. The latter may be present in the Searle-type viscometer (the inner cylinder, or bob, rotates).

The torque on the stationary cylinder and rotational velocity of the other cylinder are measured for determination of the shear stress and shear rate, needed for viscosity calculation. Once the torque T is measured, it is simple to describe the fluid shear stress $\tau_{r\theta}$ at any point with radius r between the two cylinders:

$$\tau_{r\theta} = \frac{T}{2\pi r^2 L_{\text{eff}}} \quad (1)$$

In Eq. (1), the L_{eff} is an effective length of the cylinder at which the torque is measured. In addition to the cylinder's length L_1 it takes into account the so-called end effects.^{8–11}

However, the shear rate profile, across the gap between the cylinders, depends on the relative rotational speed, radii, and the unknown fluid properties, which seems as an "open-ended" enigma. The solution of this complex prob-

lem is given elsewhere^{9,11} in the form of the infinite series. When the cup to bob radii ratio, $\delta = R_2/R_1$, is smaller than 1.2, the first three terms of that infinite series solution will effectively represent the velocity gradient (flow curve) at stationary bob location:

$$\begin{aligned} \left(\frac{dv_\theta}{dr}\right)_{R_1} &= \frac{4\pi\Omega}{1-\delta^{-2}} \left[1 + \frac{\delta^2-1}{2\delta^2} \left(1 + \frac{2}{3} \ln \delta \right) \left(\frac{1}{n''} - 1 \right) \right. \\ &\quad \left. + \frac{(\delta^2-1)}{6\delta^2} \ln \delta \left[\left(\frac{1}{n''} - 1 \right)^2 + \frac{d(1/n''-1)}{d(\log T)} \right] + \dots \right], \end{aligned} \quad (2)$$

where n'' is the slope of a logarithmic plot of torque T versus relative rotational speed $\Omega = \omega_2 - \omega_1$.

For a non-Newtonian, power-law fluid model ($n'' = n = \text{const}$; $\tau = k_1 \dot{\gamma}^n$) in simple one-dimensional flow between two vertical concentric cylinders, when the outer cylinder rotates with ω_2 around the stationary inner cylinder, $\omega_1 = 0$ ($\Omega = \omega_2 - \omega_1 = \omega_2$), the test fluid velocity and shear rate profiles are obtained from the momentum equation as

$$v_\theta(r) = \frac{R_1 \omega_2}{1 - (R_1/R_2)^{2/n}} \left[\frac{r}{R_1} - \left(\frac{r}{R_1} \right)^{1-2/n} \right] \quad (3)$$

$$\dot{\gamma}_{r\theta}(r) = r \frac{\partial}{\partial r} \left(\frac{v_\theta}{r} \right) = \omega_2 \left(\frac{2}{n} \right) \frac{1}{(\delta^{2/n} - 1)} \left(\frac{R_2}{r} \right)^{2/n} \quad (4)$$

Substituting the shear rate, Eq. (4), in the power law equation at the inner cylinder, $\tau_1 = \tau_{r\theta}(R_1) = k_1 [\dot{\gamma}_{r\theta}(R_1)]^n$, solving for ω_2 and taking the logarithm of both sides, the following equation is obtained:

$$\ln \omega_2 = \left(\frac{1}{n} \right) \ln \tau_1 + \ln \left[\left(\frac{n}{2} \right)^n \sqrt[1/k_1]{1 - \left(\frac{R_1}{R_2} \right)^{2/n}} \right], \quad (5)$$

where the torque T can be converted to stress at the bob using Eq. (1), with $r = R_1$. First, the measurements, needed to plot $\ln \omega_2$ vs $\ln \tau_1$, has to be made in the range of interest. The reciprocal of the slope of such plot is n , and then fluid consistency, k_1 , can be determined from Eq. (5).

However, there is a simpler procedure,^{10,12} also established by German standards.^{13–15} For any fluid, including non-Newtonian fluids, there is a radius at which the shear rate is virtually independent of the fluid type for a given ω_2 . This radius is, therefore, a function of geometry only. It is called the representative radius, R_R , and is determined [using Eq. (1)] as the location corresponding to the so-called representative shear stress, $\tau_R = (\tau_1 + \tau_2)/2$, the average of the stresses at the outer and inner cylinder, i.e.,

$$R_R = R_1 \sqrt{\frac{2\delta^2}{(1+\delta^2)}} = R_2 \sqrt{\frac{2}{(1+\delta^2)}} \quad (6)$$

Since the shear rate at the representative radius is virtually independent of the fluid type (whether Newtonian or non-Newtonian), the representative shear rate is calculated for Newtonian fluid ($n = 1$) and $r = R_R$, according to Eq. (4):

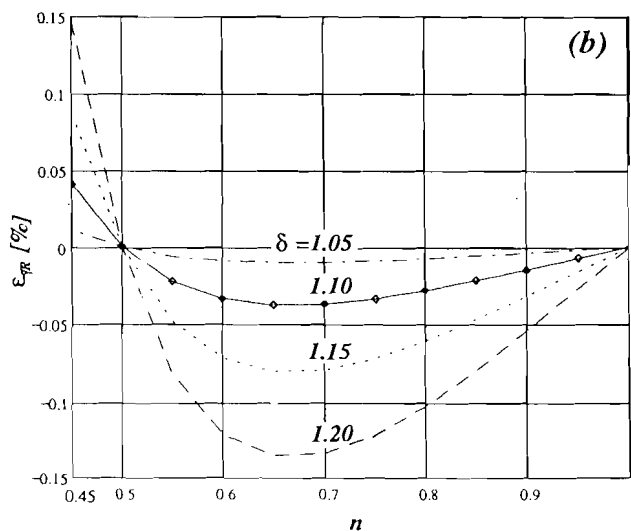
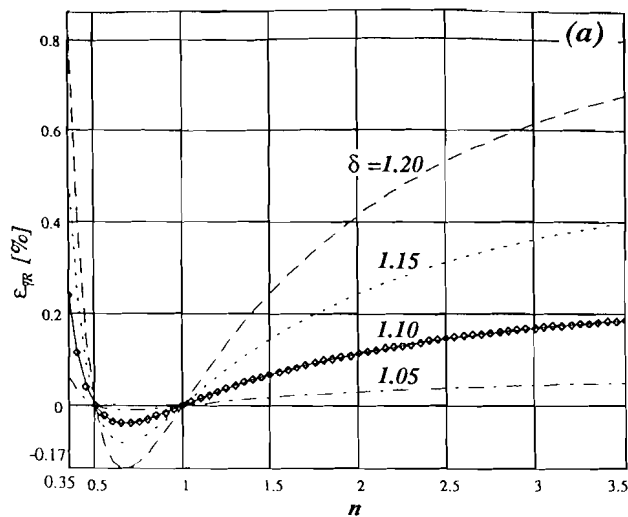


FIG. 3. Representative shear-rate errors.

$$\dot{\gamma}_R = \omega_2 \frac{(\delta^2 + 1)}{(\delta^2 - 1)} \quad (7)$$

The accuracy of the representative parameters depends on the geometry of the cylinders (δ) and fluid type (n). According to German standards,¹⁵ the radii ratio $\delta = R_2/R_1$ should be equal or less than 1.1. Actually, the error associated with the representative parameters concept is virtually negligible for practical measurements. The percentage shear rate error, defined by Eq. (8) is plotted in Figs. 3(a) and 3(b) as a function of the power-law index with the cylinders' radii ratio as a parameter:

$$\varepsilon_{\dot{\gamma}_R}(\delta, n) = \frac{\dot{\gamma}_R(\delta) - \dot{\gamma}_{r\theta}(\delta, n)}{\dot{\gamma}_{r\theta}(\delta, n)} 100\% \quad (8)$$

It is seen from Fig. 3(a) that, for an unrealistically wide range of fluid types ($0.35 < n < 3.5$) and cylinders' geometry ($\delta = 1-1.2$), the maximum errors are less than $\pm 1\%$. Actually, for our geometry ($\delta = 1.1$), the maximum errors are less than $\pm 0.24\%$. Since the vast majority of real fluids

are in the range of $0.45 < n < 1$, the actual errors are much smaller, within $\pm 0.15\%$ and $\pm 0.04\%$ for $\delta = 1.2$ and $\delta = 1.1$ (our geometry), respectively, see Fig. 3(b). Therefore, the simple concept of representative parameters works exceptionally well.

Finally, the (apparent) fluid viscosity is determined as the ratio between the shear stress and corresponding shear rate, or by using Eqs. (1), (6), and (7), as

$$\eta = \eta_a = \eta_R = \frac{\tau_R}{\dot{\gamma}_R} = \left(\frac{\delta^2 - 1}{4\pi\delta^2 R_2^2 L_{\text{eff}}} \right) \frac{T}{\omega_2} \quad (9)$$

For a given cylinder's geometry (δ , R_2 , and L_{eff}), the viscosity may be determined from the above equation by measuring the torque T and rotational speed of the outer cylinder ω_2 .

As already mentioned, in Couette-type viscometers the Taylor vortices within the gap are virtually eliminated. However, vortices at the bottom may be present, and their influence becomes important when the Reynolds number reaches the value of unity.¹⁴ Furthermore, the flow instability and turbulence will develop when the Reynolds number reaches values of 10^3-10^4 . The Reynolds number for the flow between concentric cylinders is defined¹⁴ as

$$Re = \frac{\rho\omega_2 R_1^2}{2\eta} (\delta^2 - 1) \quad (10)$$

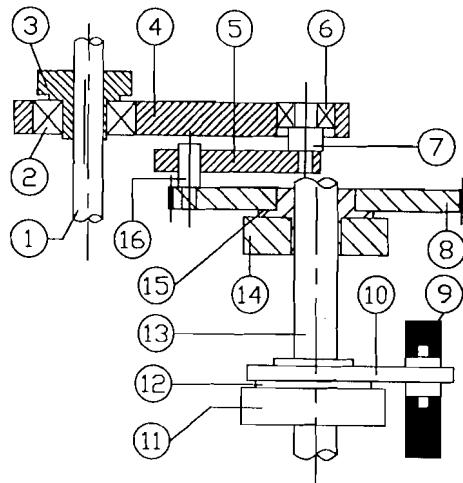
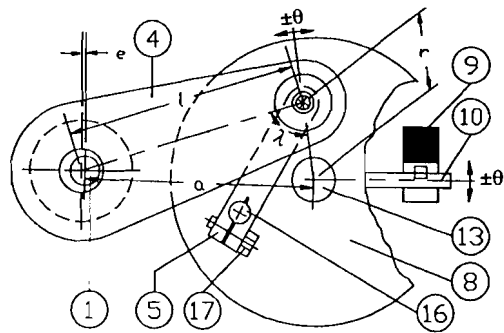
A rotational viscometer is the only viscometer capable of measuring the phase lag between stress and strain, the complex shear modulus G^* (i.e., storage G' and loss modulus G''), and the dynamic viscosity η' under simple harmonic oscillatory testing, where strain γ may be expressed as

$$\gamma = \gamma_0 \sin(2\pi f_2 t), \quad (11)$$

where f_2 is oscillatory frequency of the outer cylinder in Hz, and γ_0 is the oscillatory strain amplitude in rad, calculated as the ratio of the outer cylinder's arc amplitude and the gap thickness, i.e.,

$$\gamma_0 = \frac{\theta_0 R_2}{R_2 - R_1} \quad (12)$$

Note that θ_0 is the angular oscillation amplitude of the outer cylinder in rad. In our instrument, the oscillatory deformation is provided by the same motor used in steady-rotational mode and a special, oscillatory linkage mechanism, see Fig. 4. It is a modified "four-bar" linkage, consisting of (i) a fixed link a , between axes of shafts (1) and (13); (ii) eccentric driver-crank (3) with length e , between shaft's (1) and bearing's (2) axes; (iii) coupler (4) of length l ; and (iv) follower-rocker link r , between axes of bearing (6) and shaft (13). The follower length r and thereby amplitude of oscillation can be manually adjusted (from 1.1° to 2.6°) by loosening bolt (17) and modifying the position of the arm (5) around press-fixed pivot (16). This mechanism converts steady rotation of shaft (1) into an oscillatory motion of the outer-cylinder shaft (13). From the geometry in Fig. 4 and small approximation, the following equations are derived:



- | | |
|----------------------------|---------------------------|
| (1) DRIVING SHAFT | (10) EXTENSION ARM |
| (2) DRIVER BEARING | (11) EXTENSION ARM CLAMP |
| (3) ECCENTRIC DRIVER/CRANK | (12) EXTENSION ARM HUB |
| (4) COUPLER LINKAGE | (13) OUTER CYLINDER SHAFT |
| (5) ADJUSTING LINKAGE ARM | (14) GEAR CLAMP |
| (6) FOLLOWER BEARING | (15) GEAR HUB |
| (7) BEARING PIN | (16) FIXED PIN |
| (8) GEAR | (17) LOCKING BOLT |
| (9) OPTO-ELECTRONIC SENSOR | |

FIG. 4. Oscillatory mechanism and optoelectronic sensor.

$$\theta(t) = \theta_0 \sin(2\pi f_2 t), \quad (13)$$

$$\theta_0 \approx \frac{2el}{\sqrt{4r^2 l^2 - (l^2 + r^2 - a^2)^2}}, \quad (14)$$

where the linkage lengths are $a = 50.8$ mm (2 in.); $e = 0.79$ mm (1/32 in.); $l = 50.8$ mm (2 in.); $r = 17.8$ – 45.7 mm (0.7–1.8 in.). The latter range is due to structural obstruction and maximum stretching, which corresponds to limiting amplitude of oscillations of $\pm 2.60^\circ$ and $\pm 1.11^\circ$, respectively.

Equation (14) represents angular amplitude θ_0 , which actually varies slightly with time (during oscillation) as opposed to being a constant in pure sinusoidal oscillation. However, the departure from pure simple harmonic motion is minimized (less than $\pm 2\%$) by design¹⁶: relatively small eccentricity e , and large angle λ ($\lambda > 63^\circ$), between coupler l and follower r , as well as rather small angular amplitude itself ($1.11^\circ < \theta_0 < 2.60^\circ$). The latter translates, using Eq. (12), into the minimum and maximum strain amplitude, 0.21 and 0.50 rad, respectively.

Then, the shear strain rate is expressed as

$$\dot{\gamma} = 2\pi f_2 \gamma_0 \cos(2\pi f_2 t). \quad (15)$$

Depending on the test fluid type, the shear stress is not necessarily in phase with the shear strain nor the shear rate, i.e.,

$$\tau = \tau_0 \sin(2\pi f_2 t + \alpha), \quad (16)$$

where τ_0 is the oscillatory shear stress amplitude, and α is the phase lag (phase shift) between the shear stress and the corresponding shear strain. For an arbitrary substance the phase shift has to be between the limits of 0 and $\pi/2$ rad, the Hookean elastic solid and the Newtonian viscous fluid, respectively.^{3,17}

Finally, the real (storage) and imaginary (loss) components of the complex shear modulus G^* and the dynamic viscosity η' are defined as^{3,17}

$$G' = \Re(G^*) = \frac{\tau_0}{\gamma_0} \cos \alpha, \quad (17)$$

$$G'' = \Im(G^*) = \frac{\tau_0}{\gamma_0} \sin \alpha, \quad (18)$$

$$\eta' = \Re(\eta^*) = \frac{\tau_0}{2\pi f_2 \gamma_0} \sin \alpha. \quad (19)$$

The real component G' is in phase with shear strain and represents the elastic character of the test substance (stored energy could be recovered), hence it is called "storage" modulus. The imaginary component G'' (out-of-phase with regard to shear strain, but is "in-phase" with shear rate) represents the viscous/plastic character of the test substance and is called "loss" modulus (since energy is dissipated/lost and cannot be recovered).

Both stress and strain need to be known as simultaneous functions of time to determine the phase shift (α) between them, loss and storage moduli, and dynamic viscosity. Strain amplitude is normally set [see Eqs. (12) and (14)] to be a fraction of a radian so that the sinusoidal fluid deformation would not overcome the elastic limit of the test fluids. Stress is calculated through the torque measurement at the inner cylinder. Therefore, the measured torque is very small. To overcome this difficulty, frequency is normally increased, yet it has to remain below the natural frequency of the system. In addition to the analysis presented, two corrections need to be made: The first is in reference to strain. Equations (11) and (15) do not consider a very small rotation of the inner cylinder, due to torsion bar deformation. This small rotation (small even as compared to the small oscillation of the outer cylinder) is needed to measure torque. The second correction is in reference to the torque. Equation (1) does not include the inertial torque due to the oscillation of the torsion-bar inner-cylinder assembly and the test fluid. Therefore, a more complex model should be used for determination of the complex modulus and dynamic viscosity.

The torque magnitude [see Eq. (1)] increases with the radius to the cube (since L_1 is proportional to R_1). However, the Reynolds number also increases with the radius squared [see Eq. (10), which is undesirable], as well as cost of the components. After detailed analysis and design optimization, the following dimensions were determined (see Fig. 1):

$$\delta = R_2/R_1 = 1.1,$$

$$R_1 = 16.51 \text{ mm (0.65 in.)} = D_1/2,$$

$$R_2 = \delta R_1 = 18.161 \text{ mm (0.715 in.)} = D_2/2,$$

$$L_1 = 4R_1 = 66.04 \text{ mm (2.6 in.)},$$

$$L' = R_1 = 16.51 \text{ mm (0.65 in.)},$$

$$L'' = R_1 = 16.51 \text{ mm (0.65 in.)},$$

$$R_3 = 0.2885R_1 = 4.7625 \text{ mm (0.1875 in.)} = D_3/2,$$

$$\beta = 150^\circ.$$

For a shear rate range of interest between 1 and 200 s^{-1} , the rotational speed ($N_2 = 30\omega_2/\pi$) range, from 1 to 180 rpm, is calculated from Eq. (7). The torque range of 0.015–8.3 mNm (ratio 1/550) is calculated using Eq. (9), assuming that the thinnest fluid viscosity (0.5 mPa s) is measured at the highest rotation (180 rpm) and the thickest fluid (50 000 mPa s) at the lowest rpm. It is obvious that the measurements in a wider range of parameters would require more than one pair of cylinders and/or torque sensor. As an example, if a fluid with $\rho = 1000 \text{ kg/m}^3$ and a viscosity of 100 mPa s is tested at 100 rpm, then the Reynolds number will be 3.0 and the torque 1.65 mNm.

It is also important to estimate the torque expected to be measured in oscillatory testing. The following case illustrates that the torque magnitude in oscillatory testing is smaller than the corresponding steady shear-rate torque: If f_2 were 1 Hz and $\delta = 1.1$, then, using the above equations, the oscillatory rotational torque would equal the steady rotational torque if the amplitude of oscillation is equal to 1/11 rad (or 5.2°). However, the angular amplitude has to be smaller than this value to be within the fluid elastic deformation rate, implying a very small oscillatory torque. This example illustrates that measuring very small torque under oscillatory testing conditions is a major challenge in a rheometer design. One solution would be to increase the frequency as much as possible (to obtain a larger torque).

IV. NOVEL ALIGNMENT TECHNIQUE AND PROCEDURE

Perhaps one of the most critical factors in the operation of the viscometer is the accurate alignment of the inner and the outer cylinder. Both cylinders need to be vertical and concentric. Verticality is necessary to avoid unwanted influence of gravitational forces, and it is ensured by using a site level. No reference that specifies error (in torque measurement) as a function of verticality has been found. However, the standard¹⁴ specifies torque mea-

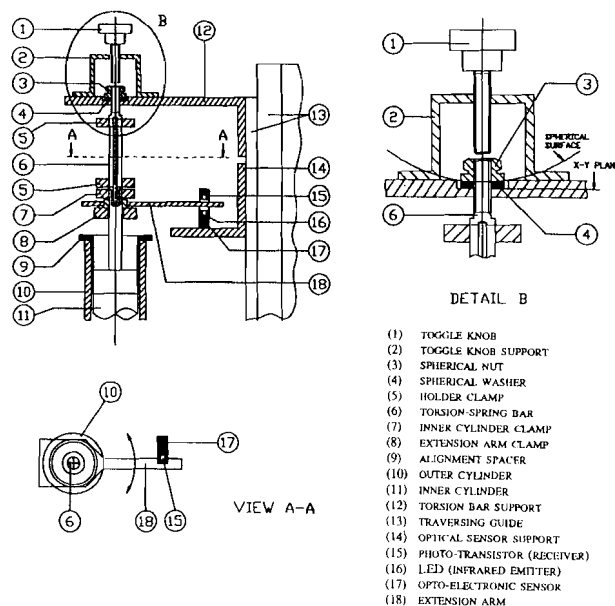


FIG. 5. Alignment and inner-cylinder torsion-bar assembly.

surement error as a function of eccentricity. The values specified refer to cylinders with parallel axes. In addition to eccentricity, the axes of the cylinders may not be parallel to each other, among other things because of rotation of the axis of the outer cylinder. This is caused by the radial clearance of the bearings, shaft bending, and manufacturing tolerances. However, for the error estimation, the lack of parallelism is treated as eccentricity.

The inner-cylinder torsion-bar assembly is depicted in Fig. 5. The whole assembly may be moved up and down along a precise traversing guide (13) in order to disengage the inner and outer cylinders. The novel alignment technique and procedure is based on aligning the free/loose torsion-bar inner-cylinder assembly i.e., setting the inner cylinder's (11) position with reference to the outer cylinder (10), by placing a precise spacer (9) between them. Once the inner cylinder is accurately positioned, the assembly is fixed by tightening knob (1). The spherical nut (3) and washer (4) would accommodate the positioning of the inner cylinder as needed, horizontal or tilting (see Fig. 5). To allow for easy adjustment, the spacer has a play of 0.076 mm (0.003 in.) with respect to the outer cylinder and 0.203 mm (0.008 in.) with respect to the inner cylinder. These plays will influence the accuracy of the alignment of the cylinders. After the inner cylinder is properly aligned with reference to the outer cylinder, and the inner-cylinder torsion-bar assembly is firmly fixed with knob (1), the inner cylinder is raised in the upper position along guide (13), and the spacer (9) is removed and saved for future realignment when and if needed.

V. NOVEL TORSION-SPRING BAR

It has already been indicated that small torque values are to be measured, particularly in the oscillatory tests. To have a measurable angular deformation, the torsion-spring bar must have a low torsional stiffness, which in turn re-

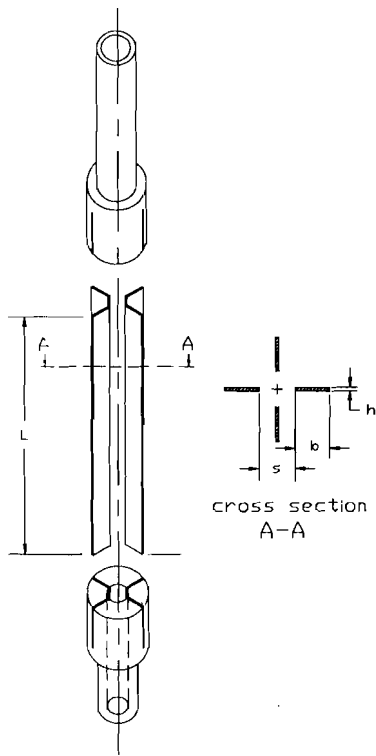


FIG. 6. Hollow-cruciform torsion-spring bar.

duces its bending rigidity and operational stability. In the commercial viscometers and rheometers, where the torsion-spring bars are usually of simple circular or rectangular cross sections, an air-bearing support between the torsion-spring bar and the inner cylinder is used, together with highly precise manufacturing tolerances, to provide alignment and stable operation of the instrument.

However, our objective was to design such a torsion-spring bar on which the inner cylinder could be freely suspended, thus eliminating the use of expensive and cumbersome air-bearing and all other disadvantages associated with it. That implies that the torsion-spring bar should have such a geometry as will provide the ratio between the bending and torsional rigidity as high as possible. The geometry selected was the hollow cruciform shape shown in Fig. 6. This geometry provides a much higher bending resistance at a given torsional rigidity as compared to the corresponding cylindrical torsion-spring bar.¹⁸

$$K = \frac{J'G}{L}, \quad (20)$$

where K the spring stiffness in N m/rad; J' the torsional rigidity factor, equal to the polar moment of inertia J in m^4 for simple cross sections; G the shear modulus of elasticity in Pa; and L length of the spring bar in m.

For other more complex cross sections, a torsional rigidity factor J' has to be defined. In the case of a cruciform chosen in our design, which consists of four rectangular element shims (see Fig. 6), the rectangular torsional rigidity factor,¹⁹ J'_R , is multiplied by 4:

$$J' = 4J'_R = 4 \frac{bh^3}{16} \left[\frac{16}{3} - 3.36 \frac{h}{b} \left(1 - \frac{h^4}{12b^4} \right) \right], \quad (21)$$

where J' and J'_R are in m^4 , and h and b , the sizes of the rectangular cross section ($b > h$), are in m. This formula represents a good agreement with the values found elsewhere.²⁰

The axial moment of inertia $I = I_x = I_y$, of the cruciform cross section is also a function of the separation displacement of the elements, s , as shown in Fig. 6:

$$I = \frac{1}{12} [2bh^3 + h(s+2b)^3 - hs^3]. \quad (22)$$

For the torsion-spring bar, the following dimensions were selected (see Fig. 6): $b = 3.048$ mm (0.12 in.); $h = 0.3048$ mm (0.012 in.); $s = 3.175$ mm (0.125 in.). Substituting these values (in SI units) in Eqs. (21) and (22), the following values are obtained for the torsional rigidity factor $J' = 107.83 \times 10^{-15} \text{ m}^4$ and bending moment of inertia $I = 19.442 \times 10^{-12} \text{ m}^4$.

Note that for a cylindrical torsion-spring bar (circular cross section of diameter d), the axial moment of inertia I and torsional rigidity J' , i.e., polar moment of inertia J are equal to

$$I = \frac{\pi d^4}{64}; \quad J' = J = \frac{\pi d^4}{32}. \quad (23)$$

The ratio I over J' is 180.3 for the cruciform, Eqs. (22) and (21); and 0.5 for any circular cross-sectional area, Eq. (23). This means that a cruciform cross section would have much higher bending resistance (≈ 360 times) than the corresponding circular cross section of the same torsional resistance. Since our torsion-spring bar is made of brass ($G = 41$ GPa) the torsional stiffness is calculated using Eqs. (20) and (21) to be $K = 0.116$ N m/rad = 116 mN m/rad. The same value of K can be obtained using a stainless-steel ($G = 73$ GPa) solid-round bar of the same length and 0.886 mm (0.035 in.) diameter. However, in this latter case, the resistance to bending would be about 360 times smaller than the cruciform's.

Obviously, fabricating the cruciform torsion-spring bar is more difficult and expensive than a cylindrical one. Figure 6 shows the major parts of the torsion-spring bar. The upper and lower holders are made of aluminum to minimize inertia, and the torsion-spring bar itself is made of brass shims, 0.304 mm (0.012 in.) thick. To ensure a correct concentricity between the top and bottom parts, a small grounded cylindrical rod 3.175 mm (1/8 in.) diameter is placed through the rimmed holes of the aluminum holders before the shims (6) are mounted in the holders' slots and tightened with the clamps (5) (see Fig. 5). Once the shims are properly aligned and mounted, the rod is taken out.

The natural frequency of the system of torsion-spring bar and inner cylinder is calculated by using

$$f_n = \sqrt{K/I_0} (1/2\pi), \quad (24)$$

with f_n in Hz, K in N m/rad, and I_0 in kg m^2 . With the values of inertia of the inner cylinder $I_0 = 13.3 \times 10^{-6} \text{ kg m}^2$ (neglecting inertia of relatively light torsion-spring

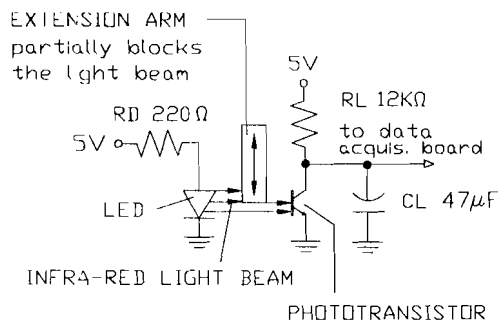


FIG. 7. Optoelectronic sensor and signal conditioning circuit.

bar, aluminum extension arm and clamps) and the spring stiffness $K=0.116 \text{ N m/rad}$, Eq. (24) gives the natural frequency of about 15 Hz, which is higher than 13.1 Hz, the measured natural frequency of the torsion-spring bar inner-cylinder assembly. In any case, the natural frequency is higher than a recommended maximum operational frequency of 10 Hz for oscillatory testing.

VI. NOVEL OPTOELECTRONIC SENSORS

In our design, the general-purpose, inexpensive optoelectronic sensors (price range around ten dollars) are utilized to measure the angular deformation of the torsion-spring bar, oscillatory displacement of outer cylinder, and even rpm of the motor. However, the most often used sensors by manufacturers of commercial viscometers are the linear variable differential transformers (LVDT). Their price ranges up to hundreds of dollars, depending on the complexity of their electronic circuitry.

The principle of work of an optoelectronic sensor is as follows, see Figs. 5 and 7: A light-emitting diode (LED) (16) sends an invisible infrared light beam that is received by a light sensing detector (15), phototransistor or photodiode. Phototransistor based detectors provide higher signal levels and therefore were selected for this project. The voltage output of the optoelectronic sensor depends on the amount of the LED's light beam which reaches the detector, i.e., on the partial blockage of the infrared light beam by the extension arm (18). However, the extension arm's light blockage (i.e., its displacement) directly depends on the torsion-spring bar deformation, which in turn, is proportional (through the spring bar stiffness) to the measured torque. The photomicrosensor model EE-SJ8-B, made by OMRON²¹ (17), was used in our design, see Figs. 2, 4, 5, and 7. It is an active photoelectronic sensor which has to be powered by 5 V dc. The signal generated by the phototransistor has to be conditioned before it can be read by the data acquisition board, millivoltmeter, or an oscilloscope.²² Additional resistors are added to limit the amount of the current through the circuit, thus minimizing the heating of the electronic elements. Schematics of the optoelectronic sensor and corresponding signal conditioning circuitry is shown in Fig. 7. A special setup, designed to calibrate precisely the optoelectronic sensor, is described later (see Fig. 8).

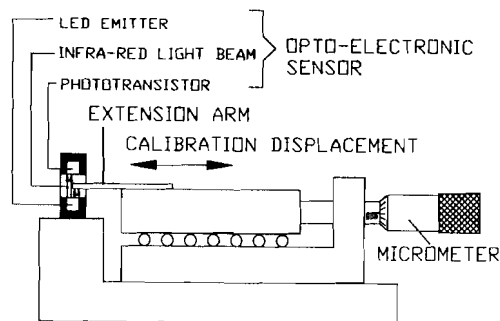


FIG. 8. Calibration setup of optoelectronic sensor.

In oscillatory testing mode, the simple harmonic motion (of small amplitude) of the outer cylinder is measured in a similar manner as the torsion spring deformation (see Fig. 4): An extension arm (10) is mounted on the shaft (13) which drives the outer cylinder, and an optical sensor (9) (the same model as one used in the torque measurements) is so positioned as to detect the extension arm's displacement. It is more convenient for installation and calibration to have the same type of optical sensors for both stress and strain measurements. The difference in ranges is compensated for by adjusting the lengths of the corresponding extension arms.

Even the motor's rotational speed (rpm) is measured with the same type of optoelectronic sensor (see Fig. 2). This time, for every revolution of the motor, a special arm mounted on its shaft interrupts the sensor's infrared beam, thus sending electrical pulses to the data acquisition board and PC.

VII. DATA ACQUISITION AND SOFTWARE

The instrument operation and data reduction are computerized by using a commercial, general-purpose data acquisition board and an IBM-compatible PC. A specially designed software is responsible for communication between the computer and the sensors through the data acquisition board. The software also interprets and reduces the data, to calculate viscosity and phase lag between stress and strain, for example. The software was written in C programming language, which is a convenient language for communication with electronic signals, data acquisition, and computer hardware.

The data acquisition board is model ADA2000, manufactured by Real Time Devices, Inc.²³ The analog voltage coming from the optical sensor used in the torque transducer is read by one of the 16 analog inputs. The analog voltage coming from the optical sensor used to measure the oscillatory displacement is read by another analog input. The digital signals (pulses) generated by the rotational velocity sensor go directly (passing through the data acquisition board) to the CPU of the PC generating a hardware interrupt. After analyzing the data, an appropriate analog signal is sent to control the motor's velocity by varying its voltage source level.

The inertia of the moving driving parts, principally the inertial torque in the motor's rotor, will reduce any unde-

sirable mechanical noise effect. Even in oscillatory motion, because of the large transmission ratio, the oscillatory forces are negligible as compared to the inertial forces on the motor shaft. In general, the forces to be overcome by the motor should not affect its behavior. Therefore, a proportional control was chosen for the velocity control. Nevertheless, for viscosity or elasticity properties measurement, a precise velocity measurement is far more important than a precise velocity control. The apparent viscosity can be calculated accurately for any set velocity as long as the actual velocity is measured accurately and used in the calculations.

Viscosity is determined using Eq. (9). The rotational velocity of the outer cylinder is calculated by measuring the velocity of the motor N_m and multiplying this value by the appropriate transmission factor. The torque T is calculated using the calibration results [see Eqs. (27) and (28) in the next section], and by measuring the corresponding voltage V_{ts} generated in the optical sensor. Then, from Eq. (9) taking into account the above, the working viscosity expression is

$$\eta_a = \left(\frac{15(\delta^2 - 1)}{2\pi^2\delta^2} \frac{K}{L_{\text{arm}}R_2^2L_{\text{eff}}} 10^9 \right) \frac{f(V_{ts})}{N_2}, \quad (25)$$

where η_a in mPa s; N_2 in rpm; R_2 , L_{eff} , and L_{arm} in mm; K , torsional stiffness in mNm/rad; and $f(V_{ts})$, displacement as a function of the sensor's voltage in mm [Eq. (28)].

In actual measurements, the velocity of the motor and the voltage of the torque transducer are measured several (5) times at a high sampling rate. Standard deviations of errors are combined to calculate viscosity precision error as shown:

$$\varepsilon_{\eta} = \sqrt{[(1/\dot{\gamma})\varepsilon_r]^2 + [(\tau/\dot{\gamma}^2)\varepsilon_v]^2}. \quad (26)$$

A simultaneous, real-time measurement of both the rotational position of the outer cylinder (fluid strain) and the output voltage of the torque transducer (fluid stress) is needed to determine the phase shift between stress and strain. The signals' data may be represented (approximated) by simple harmonic functions, see Eqs. (11), (15), and (16). Because noise is inevitable, a filter could be required. The data are stored in the ASCII format and can be further analyzed using curve fitting and/or the FFT techniques, which are conveniently available in commercial mathematical software packages, like MathCAD or MATLAB for example.

VIII. CALIBRATION AND TESTING

The instrument calibration and testing included verification of the dimensions of the cylinders, measurement of the alignment of the cylinders, comparison of the velocity measurement with a function generator signal, testing and calibration of the optical sensors, and finally, overall calibration of the viscometer against standard fluids of known viscosities.

TABLE I. Comparison between designed and actual cylinders' dimensions.

	Inner diameter of outer cylinder D_2 , mm (in.)	Outer diameter of inner cylinder D_1 , mm (in.)	$\delta = D_2/D_1$
Designed	36.32 (1.430)	33.02 (1.300)	1.100
Fabricated	$36.43 \pm 4.3E-3$	$33.27 \pm 5.3E-3$	± 1.094
% error	± 0.17	$0.75 \pm$	± 0.57

A. Dimensions and alignment

The diameters of the cylinders were verified after their fabrication. Comparison between the designed and the manufactured dimensions for both cylinders is presented in Table I.

As mentioned before, perhaps one of the most critical parts in the operation of the viscometer is the correct alignment of the inner and the outer cylinder. Results are presented in Table II. The results in Table II were obtained through piece-by-piece measurements. During normal operation, the test fluid flow would tend to self-align the cylinders. Therefore, the actual error will be smaller than anticipated.

B. Torque transducer

It is quite reasonable to assume that the relationship of the torque versus angular deformation is linear, because the torsion-spring bar deformations are designed to be well within the elastic range. Still, any nonlinearity was checked out by the overall calibration of the viscometer/rheometer using the standard fluids of known viscosities.¹⁸ It was indicated in previous sections that the measured torque T is directly related to the extension arm's displacement, i.e., infrared light beam blockage $d_x = f(V_{ts})$, which is in turn measured by the output voltage V_{ts} , generated in the optoelectronic sensor:

$$T = K\theta_1 = K \frac{d_x}{L_{\text{arm}}} = K \frac{f(V_{ts})}{L_{\text{arm}}} = \text{function}(V_{ts}), \quad (27)$$

where the stiffness K is determined by Eqs. (20) and (21) using the known shear modulus of elasticity G for the material of the torsion-spring bar. The functional relationship $d_x = f(V_{ts})$, not necessarily linear, has to be determined by calibration [see Eq. (28)] since the spring stiffness K and the arm's length L_{arm} are known constants for a given design of the torque transducer.

TABLE II. Cylinders' alignment.

Eccentric rotation of outer cylinder (mm)	top	0.216
	middle	0.140
	bottom	0.063
Radial play of spacer (mm)	with outer cylinder	0.038
	with inner cylinder	0.102
Eccentricity at middle of cylinder (mm)		0.239
Eccentricity allowed for torque measurement (Ref. 15) (mm)	for 0.5% error	0.124
	for 1% error	0.165
	for 2% error	0.231

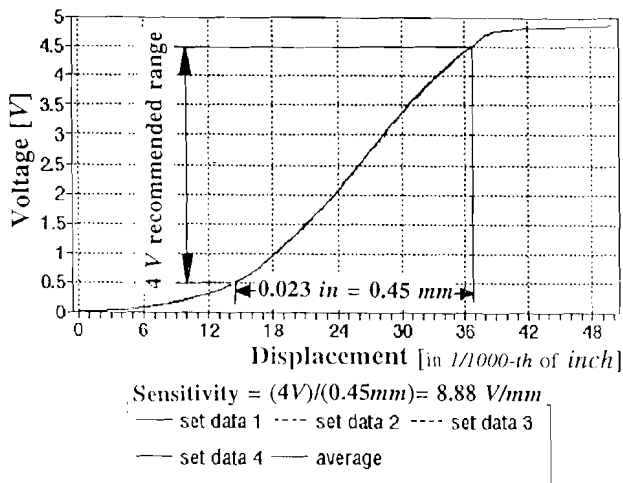


FIG. 9. Calibration curve of optoelectronic sensor.

A ball-bearing micrometer-positioning setup was designed and used for calibration of the optoelectronic sensor, see Fig. 8. An extension arm, of the same material and dimensions as the actual one, was mounted on a traversing mechanism. Using the micrometer, the extension bar could accurately be positioned (resolution 0.001 in. or 0.0254 mm) between the LED emitter and phototransistor of the photoelectronic sensor, thus, simulating actual measuring conditions.

The final calibration results are presented in Fig. 9. Four sets of data were collected moving the extension arm in increments of 0.001 in., two times forward and two times backward, in order to investigate hysteresis and repeatability of the sensor. From Fig. 9 it may be concluded that the sensor's static sensitivity is almost linear in the range between 0.5 and 4.5 V (corresponds to displacement range of 15–37 thousands of an inch). Note that the sensitivity outside this range is small and unreliable. Still, to increase accuracy, a cubic polynomial was chosen to curve fit the calibration data using the least-squares method. The following equation was obtained:

$$d_x = f(V_{ts}) = 0.0254(a_0 + a_1 V_{ts} + a_2 V_{ts}^2 + a_3 V_{ts}^3), \quad (28)$$

where the extension arm's displacement arc length, d_x , is in mm, the torque sensor's output voltage, V_{ts} , is in V, and coefficients a_i 's and their standard errors are given in Table III. The correlation coefficient of the calibration curve, Eq. (28), is virtually unity due to high precision and repeatability of the optoelectronic sensor.

TABLE III. Calibration coefficients of optoelectronic sensor.

Curve-fit coefficients, Eq. (28)		
	Value	Std. error
a_0	10.24891	0.031514
a_1	9.678188	0.083781
a_2	-1.97519	0.036728
a_3	0.249974	0.004765
Correlation coeff.	0.99999	
No. of points	23	

TABLE IV. Viscosity measurement: 51.0 mPa s standard fluid calibration.

No.	N_2 (rpm)	$\dot{\gamma}_R$ (s^{-1})	τ_R (mN/m^2)	η (mPa s)	SD% (%)
11	18.348	21.513	1141.344	53.055	0.33
12	29.788	34.926	1835.672	52.560	0.23
13	30.276	35.498	1909.129	53.781	0.23
14	30.224	35.437	1837.433	52.866	0.30
15	40.697	47.716	2506.693	52.534	0.18
16	41.172	48.273	2474.273	51.256	0.41
17	41.076	48.160	2521.604	52.358	0.36
18	64.748	75.915	3805.914	50.134	0.46
19	64.554	75.687	3741.136	49.429	0.19
20	51.767	60.696	3122.804	51.450	0.27
21	52.101	61.087	3108.962	50.894	0.35
22	52.897	62.020	3168.056	51.081	0.19
23	53.807	63.087	3221.519	51.065	0.19
24	84.534	99.113	4855.117	48.986	0.36
25	84.240	98.769	4885.628	49.465	0.34
26	85.277	99.985	4887.237	48.880	0.26
27	84.460	99.027	4857.521	49.052	0.42
28	135.420	158.776	7925.932	49.919	0.41
29	135.043	158.334	7881.153	49.775	0.75
30	135.608	158.996	7877.216	49.543	0.26
31	136.180	159.667	7924.611	49.632	0.52

C. Overall calibration with standard-viscosity fluids

Previously, the ideal mathematical formulation simplifying real conditions was given. However, ideal conditions do not occur in real instrumentation/processes. There are always some additional, undesirable effects to be taken into account. One of them is the torque exerted by the fluid at the bottom and top of the inner cylinder. An additional effect is due to secondary flow at the bottom of the cylinders. These effects are proportional to the velocity and normally are taken into account by adding a correcting length to the actual length L_1 of the inner cylinder. When the Reynolds number exceeds the value of unity, the secondary flow effects are no longer proportional to the velocity, and the linearity is lost. A detailed explanation of the corrective factors are described in DIN¹⁴ 53018, Part 2.

Table IV presents viscosity measurement results for a standard fluid of 51.0 mPa s (at 25 °C). Each viscosity is calculated by measuring the rotational velocity and torque several (five) times. The mean value is then printed as well as the standard deviation (SD), calculated by Eq. (26), combining the standard deviations of both velocity and torque. The rotational speed of the motor was virtually constant during operation. Still, some very low amplitude and noisy oscillations were detected in steady rotational mode [see Fig. 10(a)]. The frequency of these oscillations matches the rotation of the outer cylinder. The cause of this "noise" may be variations in viscous torque due to the cylinders' eccentricity, deformation of the shaft which may cause different friction torque in the bearings, and/or eccentricity of the gears which may cause a different torque needed to drive the outer cylinder.

D. Oscillatory tests

The oscillatory mechanism was tested by using Newtonian standard fluids of 51.0 and 445 cP. In addition, a

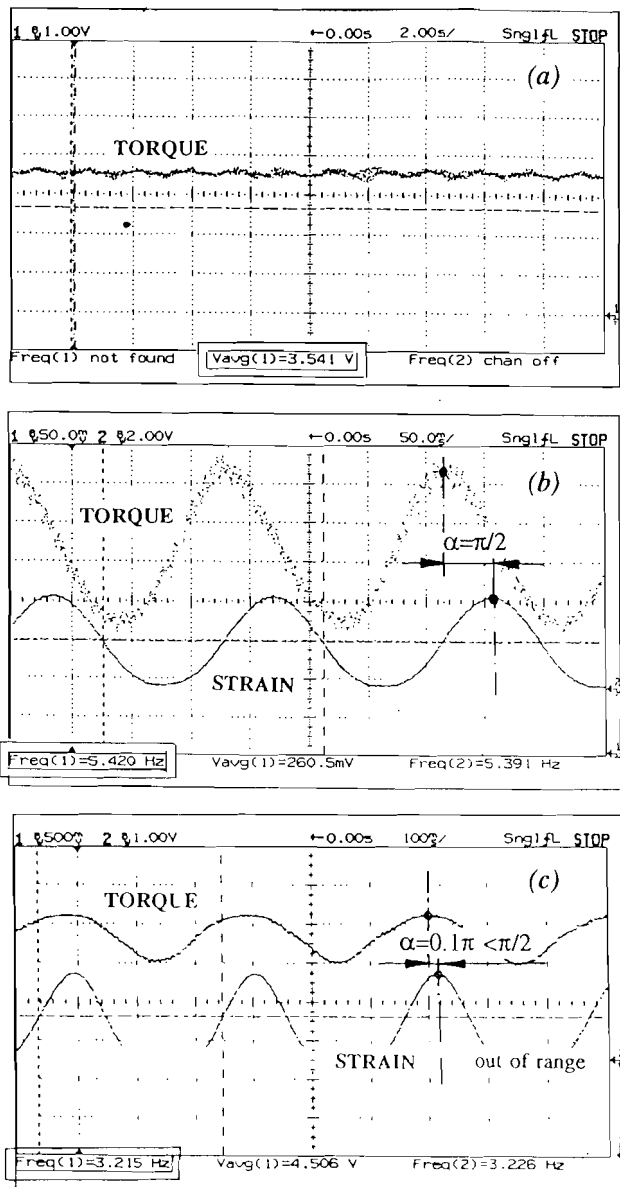


FIG. 10. Oscilloscope measurement samples.

viscoelastic fluid, 0.1% polyacrylamide aqueous solution (Praestol 2530, manufactured by Stockhausen) was tested.¹ These results show the behavior of the instrument under oscillatory deformation tests. Room temperature was 23 °C for the 51.0 mPa s standard fluid, and 25 °C for the 445 mPa s standard fluid and Praestol viscoelastic solution. The fluids were tested at different strain amplitudes (0.20–0.48 rad) and frequencies (1–10 Hz). Some characteristic test results are presented in Figs. 10(b) and 10(c).

IX. RECOMMENDATIONS

An innovative, Couette-type viscometer/rheometer was developed, designed, and fabricated with the main objective to measure viscosity and elastic properties of low-viscous, non-Newtonian, and viscoelastic fluids, like dilute polymer solutions. The goal was to simplify and improve some existing drawbacks of commercial instruments em-

ploying several novel design solutions, particularly with regard to instrument precision and sensitivity. The innovative design solutions (use of a cruciform torsion bar, optoelectronics sensors, and a novel alignment procedure) have improved the critical instrument performance and reduced the number and cost of components, customarily used in commercial viscometer/rheometers. With a single pair of cylinders and a torsion bar stiffness of 0.116 Nm/rad, viscosities from 0.5 to 50 000 cP in a shear-rate range from 1 to 200 s⁻¹, and oscillatory tests from 0.1 to 10 Hz, could be measured. The transducers' electronic signals are handled by a developed software in C language and an IBM-compatible personal computer with a data acquisition board.

The cylinders were manufactured precisely (Table I), and the diameter ratio of 1.1 is within the range specified by the standards. However, the eccentric rotation of the outer cylinder (Table II) indicates that an error of about 2% in torque measurement could be expected. However, this error would be smaller during normal operation when the test fluid flow would tend to self-align the two cylinders. Mechanical noise was reduced to a very small level by using a rubber timing belt and rubber pads in critical support parts. A simple signal filter has virtually eliminated all high-frequency noise for steady shear rate viscosity measurements.

Velocity measurements were highly accurate (estimated error of less than 0.3%). However, the open-loop velocity control circuit was unstable and needs to be improved. Temperature effect on the motor's coil and electronic driver may influence instability. Therefore, the control circuit was not used and the motor's velocity was varied by changing manually the voltage of the power supply. Nevertheless, the rotational speed of the motor was virtually constant during operation. Improvement may be achieved by adding a closed-loop velocity control feature to the electronic circuit. A simpler (and probably better) solution would be to use a bigger motor and a bigger flywheel. The fact that a bigger motor may be required is also inferred by the inability of the motor to operate stably at the outer cylinder's velocities smaller than 3 rpm. Even in the range up to 10 rpm, the lack of steady velocity may be noticed. This additional problem at lower speeds is caused by the inherited low power of this type of motor at low rpm, regardless of the transmission. The error due to the velocity oscillation was minimized by the fact that the torque and corresponding velocity are measured virtually simultaneously.

The torque-deformation relationship of the torsion-spring bar was assumed linear (very small deformation, well within the elastic limit). The optoelectronic sensor was calibrated, and the results are shown in Fig. 9. The results show high repeatability at almost all ranges. However, only the central range was utilized where the sensitivity was highest. Approximately 30 s was required for the sensor's warm-up to allow its electronic components to reach an equilibrium temperature. All tests were done at about 25 °C (room temperature). No tests of temperature effect on the optical sensor were performed. Also, the aging

effect on the sensor's characteristics (during its lifetime) has to be investigated. Although the sensor uses infrared light, it may have some sensitivity to visible light. To minimize the effects of external light, the receiver (phototransistor) is mounted on the top, and the infrared emitter (LED) at the bottom, of the sensor's gap. More experiments to detect the effects of external light sources on the sensor may be performed. Because of all those influencing factors on the sensor's characteristics, *a periodic recalibration is recommended under the same conditions (external lighting, etc.) as anticipated for the actual tests.*

The alignment proved to be more difficult to achieve than expected. The friction between surfaces of the support, spherical nut and washer, somehow limits the parts to slide and self-adjust freely. These surfaces should be polished and even slightly lubricated. Material with lower coefficient of friction like Teflon may be tried. More tests are needed to confirm accuracy and repeatability of the instrument over its full range of operations. They may be done using the developed procedures as soon as needed and/or new funding is available. To improve the rotational velocity control and stability at lower velocities, a more efficient, feed-back closed-loop circuitry, and more powerful motor are desired. The use of one pair of cylinders and one torsion bar limits the range of operations of the viscometer. More cylinders and additional torsion bars may easily be fabricated to increase the viscosity measurement range. The design has considered the future addition of a thermal bath. Temperature measurement and control would enable fluid testing at different temperature levels.

The overall, steady shear-rate calibration was performed using the standard-viscosity fluids of 51 and 445 mPa s (or cP). Initial results show high precision, particularly at higher velocities. The oscillatory testing was performed by measuring the phase shift between the stress and strain for viscoelastic fluids and for the limiting case of a standard Newtonian fluid. The novel design has proved efficient and with potential for further improvements. On the basis of the calibration errors and the manufacturers' specifications of the transducer's components, the overall precision of the torque transducer is projected to be within $\pm 2\%$ and overall rheometer precision, within $\pm 4\%$. Overall, the results were satisfactory under most circumstances. The innovative design of the torque sensor has been proven to work beyond original expectations. The optoelectronic sensors are very cost effective and have several advantages to the LVDTs. They are absolutely nonintrusive and do not require any mechanical linkages in addition to the fixed extension arm. In the opinion of the authors, even a commercial rheometer may be feasible as a result of this research project.

ACKNOWLEDGMENTS

We would like to acknowledge the financial support by AMOCO Research and Development, Naperville, IL, and by the Committee for the Improvement of Education of Northern Illinois University (NIU), DeKalb, IL. We would like to extend our special appreciation to Dr. Parviz Payvar, Chairman of the Department of Mechanical Engi-

neering at NIU, for providing continued support, including financial, during the course of this project. We would also like to acknowledge Dr. Jim Papadopoulos for his ideas and advice in the mechanical design, as well as Mr. Al Metzger and Mr. Steve Wiora, who fabricated most of the instrument's components.

NOMENCLATURE

D_1	inner cylinder diameter
D_2	outer cylinder diameter
D_s	shaft diameter of inner cylinder
G	shear modulus of rigidity
G^*	complex modulus
G'	storage modulus
G''	loss modulus
I	area moment of inertia
I_0	mass polar moment of inertia
J	polar moment of inertia
J'	torsional rigidity factor
K	torsion-spring bar stiffness
L	torsion bar length
L_1	length of inner cylinder
L_{arm}	length of extension arm used with opto-electronic sensors
L_{eff}	effective length of inner cylinder
L'	length below inner cylinder
L''	length of test fluid above inner cylinder
N_2	rotational velocity of outer cylinder in rpm
N_m	rotational velocity of the gear motor in rpm
Re	Reynolds number
R_1	radius of inner cylinder
R_2	radius of outer cylinder
R_R	representative radius
R_s	shaft radius of inner cylinder
SD	standard deviation
T	torque
V_{ts}	voltage generated by opto-electronic sensor
a	fixed link length in oscillatory mechanism
$a_0, a_1,$ a_2, a_3	calibration coefficients of optical sensor
b	dimension in torsion bar
d	diameter of cylindrical torsion bar
d_x	extension arm's displacement arc length
e	eccentricity in oscillatory mechanism
f_2	oscillatory frequency of outer cylinder
f_n	natural frequency
h	dimension in torsion bar
k_1	power-law model consistency
l	coupler length in oscillatory mechanism
n	power-law model index
n''	slope of logarithmic torque versus rotational speed curve
r	follower length in oscillatory mechanism
r, θ	cylindrical coordinates
s	separation distance of torsion bar elements
t	time
v_θ	test fluid velocity in gap
α	phase shift between stress and strain
β	cone angle of inner cylinder

γ	shear strain
γ_0	amplitude of oscillatory strain
$\dot{\gamma}$	shear rate
$\dot{\gamma}_R$	representative shear rate
δ	radii ratio of outer and inner cylinders
$\epsilon_{\dot{\gamma}R}$	representative shear-rate error
$\epsilon_{\dot{\gamma}}$	shear rate error
ϵ_{τ}	shear stress error
ϵ_{η}	viscosity error
η	viscosity
η^*	complex viscosity
η'	dynamic viscosity
η_a	apparent viscosity
η_R	apparent viscosity at representative radius
θ	oscillatory angular motion
θ_0	angular amplitude of oscillatory motion
λ	angle between follower and coupler in oscillatory mechanism
ρ	fluid density
τ	shear stress
τ_0	amplitude of oscillatory shear stress
τ_R	representative shear stress
τ_1	shear stress at inner cylinder surface
ω_1	angular velocity of inner cylinder
ω_2	angular velocity of outer cylinder
Ω	relative angular velocity between cylinders

¹J. A. Jimenez, M. S. thesis, Northern Illinois University, DeKalb, IL, 1992.

²M. Kostic, Final report on research project, Submitted to sponsors: AMOCO Research Center, Naperville, IL; and Committee for the Improvement of Education, Northern Illinois University, DeKalb, IL, 1992.

³M. Kostic, in *Fundamentals of Heat Transfer in Non-Newtonian Fluids-*

HTD, Vol. 174 edited by J. S. N. Chen and M. A. Ebadian (ASME, New York, 1991), pp. 41-44.

⁴M. Kostic and S. Hussain, The 2nd World Conference on Experimental Heat Transfer, Fluid Mechanics and Thermodynamics, Dubrovnik, Yugoslavia, 1991.

⁵M. Kostic and J. P. Hartnett, *ZAMM J. (Z. Angew. Math. Mech., German Academy of Sciences)*, **66**, T239 (1986).

⁶J. P. Hartnett and M. Kostic, *Advances in Heat Transfer* (Academic, London, 1989), Vol. 19, pp. 247-356.

⁷T. J. E. Miller, *Brushless Permanent-Magnet and Reluctance Motor Drives* (Monographs in Electrical and Electronic Engineering N 21) (Oxford University, New York, 1989).

⁸P. Sherman, *Industrial Rheology* (Academic, London, 1970).

⁹J. R. Van Wazer, J. W. Lyons, K. Y. Kim, and R. E. Colwell, *Viscosity and Flow Measurement* (Wiley, New York, 1963).

¹⁰G. Schramm, *Introduction to Practical Viscometry* (Buchler Instruments, Frankfurt, 1987).

¹¹A. H. Skelland, *Non-Newtonian Flow and Heat Transfer* (Wiley, New York, 1984).

¹²H. Geisekus and G. Langer, Die Bestimmung der wahren Fließkurven nicht-newtonischer Flüssigkeiten und plastischer Stoffe mit der Methode der repräsentativen Viskosität, *Rheologica Acta*, Vol. 16, No. 1, pp. 1-22, January/February 1977.

¹³DIN 53018 Part 1 (German National Standard).

¹⁴DIN 53018 Part 2 (German National Standard).

¹⁵DIN 53019 Part 1 (German National Standard).

¹⁶M. Kostic, (unpublished).

¹⁷K. Walters, *Rheometry* (Chapman and Hall, London, 1975).

¹⁸M. Kostic and J. A. Jimenez, FED Vol. 161, *Fluid Measurement and Instrumentation* (ASME, New York, 1993), pp. 113-120.

¹⁹R. C. Juvinall and K. M. Marshek, *Fundamentals of Machine Component Design* (Wiley, New York, 1991).

²⁰A. P. Boresi and O. M. Sidebottom, *Advanced Mechanics of Materials* (Wiley, New York, 1985).

²¹Photomicrosensors, Cat No. X36-E1-8B, OMRON Electronics SA, Inc., Schaumburg, IL, 1988.

²²J. A. Jimenez, Project Report ELE 580-Microprocessors, Sensors, and Control Systems (graduate course), Northern Illinois University, DeKalb, IL, December 1991.

²³ADA2000 User's Manual, Real Time Devices, Inc., State College, Pennsylvania, 1990.